Comparison of Low- and Medium-Energy Collimators for SPECT Imaging with Iodine-123-Labeled Antibodies

Daniel J. Macey, Gerald L. DeNardo, Sally J. DeNardo, and Horace H. Hines

Division of Nuclear Medicine, University of California Davis Medical Center, Sacramento; and ADAC Laboratories, San Jose, California

The planar and single photon emission computed tomography (SPECT) imaging performance of two low-energy and one medium-energy collimators has been compared for ^{123}I(p,5n). Septal penetration in the low-energy collimators affected the planar uniformity and sensitivity and made the usual uniformity correction methods inappropriate. SPECT uniformity and resolution were also distorted by these artifacts induced in the planar images obtained with the low-energy collimators. The planar and SPECT images of a SPECT phantom contradicted the spatial resolution measurements made with a line source in air. The medium-energy collimator is recommended for imaging ^{123}I(p,5n)-labeled antibodies in patients, particularly when quantitation is required.

L̲ow-energy collimators have been found to be unsuitable for planar organ imaging with ^{123}I(p,2n) because of the presence of radionuclide contaminants, e.g., iodine-124 and iodine-126 that emit photons of energy greater than 200 keV. On the other hand, the same collimators have been found to yield satisfactory images of small, shallow organs, such as the thyroid with ^{123}I(p,5n) (1,2). A figure of merit approach to the same imaging problem, however, concluded that the medium-energy collimator provided a better detected signal for ^{123}I(p,5n) (3). For single photon emission computed tomography (SPECT) of the brain with iodine-123 (^{123}I) a high-resolution, low-energy collimator was considered to be marginally superior to a medium-energy collimator (4).

Iodine-123 emits a small proportion of photons with energy exceeding 400 keV; relative to the 159 keV photons, 2.4% are emitted between 440 and 625 keV, 0.15% between 625 and 784 keV. The relative influence of these photons is amplified by the increased transparency of the low-energy collimators to photons of greater energy. This septal penetration leads to a significant increase in the apparent sensitivity of the low-energy,

collimator-gamma camera combination and disturbs images of large volume sources in the body. The distance and volume of the source and the thickness of tissue around it can also modify sensitivity. Large volume sources and large amounts of surrounding tissue increase the proportion of scatter due to high-energy photons and the attenuation of the 159 keV photons. The result is an increase in the number of high-energy photons that are scattered and accepted by the photopeak window with a corresponding decrease in the proportion of primary, full-energy photons detected in the photopeak window.

The objective of this study was to compare the imaging performance of two low-energy collimators and a 300-keV, medium-energy collimator designed for gallium-67 (^{67}Ga) and to choose the optimum collimator for planar and SPECT imaging of ^{123}I(p,5n)-labeled antibodies in patients. The performance of each collimator was characterized by comparing gamma-ray spectra, planar and SPECT resolution, and sensitivity for small and large volume sources of ^{123}I(p,5n).

MATERIALS AND METHODS

The three collimators compared in this report were standard, commercially available accessories for a large field-of-view, single detector gamma camera (0.25-in.-thick NaI crystal) designed for SPECT*. Some of the

TABLE 1
Physical Characteristics of Collimators Evaluated in this Study (5)

	Energy (keV)	No. holes	Hole length (mm)	Septal thickness (mm)	Effective hole diameter (mm)
LEAP (low energy, all purpose)	140	54,600	23.6	0.18	1.409
LEHRP (low energy, high resolution)	140	81,700	23.6	0.15	1.066
300 keV (medium energy)	300	5,200	49.5	1.32	3.541

pertinent physical characteristics of these collimators are given in Table 1 (5). The gamma camera was interfaced to a nuclear medicine computer system[†] for data acquisition. A 20% energy window on the 159 keV photopeak was used for all the imaging in this report. All planar and SPECT images were acquired using either a 64 × 64, 96 × 96 (Zoom 1.5 of 64 × 64), or 128 × 128 matrix. (The 96 × 96 matrix was used for SPECT resolution measurements because the 128 matrix could only acquire in byte mode.)

For SPECT imaging, all the projection data were acquired in the step and shoot mode with either 64 or 128 views over 360° rotation. All the transverse section images were reconstructed with an array processor based computer system[‡] using a filtered backprojection algorithm and a correction for the predetermined error in the axis of rotation. A Butterworth filter with a cutoff of 0.85, the Nyquist frequency, and an order of 20 was used for the 64 × 64 matrix images: these values were 0.65 and 14 for the 96 × 96 matrix and 0.45 and 7 for the 128 × 128 matrix. The reconstructed transverse section images were 6 mm, 4.5 mm, or 3 mm in thickness for the 64 × 64, 96 × 96, or 128 × 128 matrix, respectively.

A first-order postprocessing attenuation compensation method was available for correction of the transverse section images reconstructed in this report (6). A linear attenuation coefficient (LAC) value of 0.12 cm^{-1} was used for attenuation correction if applied. The boundary of the section images could be readily defined for attenuation compensation since the SPECT phantom filled with radioactivity was of known diameter. No camera field uniformity correction was applied since section images of the SPECT phantom filled with technetium-99m indicated no significant artifacts.

Gamma-ray spectra of the photons detected by the camera for ^{123}I(p,5n) in the SPECT phantom and a 10-ml spherical source were recorded with the computer system by routing the Z signals from the camera in spectrum analysis mode to the X input of the processor analog to digital convertor.

Line sources of ^{123}I(p,5n) used for measurements of the planar and SPECT resolution in air were made with 3-cm-long microbore capillary glass tubes of 1 mm internal diameter. For planar measurements the line source was supported in air parallel to the X or Y axis

of the camera and at various distances from the collimator. For SPECT resolution the line source was placed at the center of rotation, and SPECT images acquired at various radii of rotation over 360°. All the spatial resolution measurements were made by fitting a Gaussian to the count profiles of the live source imaged in planar and transverse section images.

The SPECT phantom[§] with solid rods of lucite 4.8 to 12.7 mm diameter was filled with a solution of 6 mCi ^{123}I(p,5n). Planar images of the lucite rods in the phantom were acquired with 10^6 counts by placing the rod end of the SPECT phantom directly on each collimator. Planar images of the SPECT phantom with 10^6 counts were also acquired with the long axis of the phantom 20 cm from each collimator and aligned parallel to the collimator surface. A disk of lead 4 cm diameter and 3 mm thick (~ ten half value layers for the 159-keV photons) was placed directly on the collimator surface to cover a 12.6 cm^2 area of the uniform region of the SPECT phantom.

The SPECT resolution and uniformity for each collimator was assessed qualitatively by examining the transverse section images of the lucite rods and the uniform area of the SPECT phantom filled with ^{123}I(p,5n). Identical acquisition parameters were used for each collimator with a radius of rotation of 20 cm. No attenuation compensation was used because a count profile across the diameter of the section images obtained with the low-energy collimators did not display the anticipated reduced central count density.

The planar sensitivity of each camera-collimator combination for ^{123}I(p,5n) was determined for both a 10-ml volume source and the SPECT phantom source. The source to camera distance was 10 cm for each measurement. The gamma-ray spectra recorded for both sources with each camera collimator combination was analyzed by defining the "full-energy" peak events as the counts above a background line drawn by linear interpolation (Fig. 1). The counts in the area above this interpolation line were assumed to be 159 keV "peak" events while those in the area below the line were considered as background for sensitivity measurements. The background counts are contributed by a variety of photon interactions with the camera crystal and collimator due to septal penetration from high-energy photons and Compton scatter. Defined in this manner the
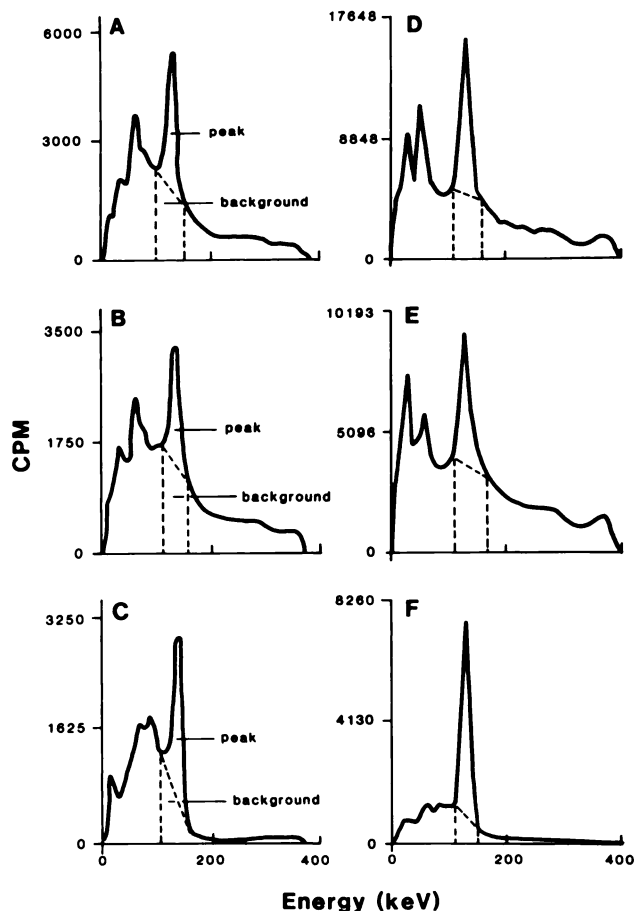
FIGURE 1
Gamma-ray spectra recorded for ^{123}I(p,5n) first in SPECT phantom using (A) LEAP, (B) LEHRP, (C) 300-keV collimator; second in 10-ml source using (C) LEAP, (D) LEHRP, and (E) 300-keV collimator. Peak and background areas for photopeak of each spectrum were defined by linear interpolation of counts in channel numbers equivalent to 127 and 181 keV limits of 20% energy window on 159-keV peak. Spectra from 300 keV had less background noise throughout energy range

RESULTS

The gamma-ray spectra recorded with the three collimators for the SPECT phantom filled with^{123}I(p,5n) are shown in Fig. 1. The spectrum obtained with the 300-keV collimator had the most symmetric photopeak and the best peak to background ratio, and it also demonstrated the lowest apparent and corrected sensitivity (Table 2).

The planar full width at half maximum (FWHM) values measured for ^{123}I(p,5n) in air using a 64 × 64 matrix and a 128 × 128 matrix for source to collimator distances of 0 to 30 cm are shown in Fig. 2. A significant improvement in the planar spatial resolution was indicated for images recorded with a 128 × 128 matrix for all three collimators. The degradation in spatial resolution with increasing source to detector distance was most marked for the 300-keV collimator which has the poorest overall spatial resolution. The SPECT FWHM values for each collimator measured with the line source of ^{123}I(p,5n) and varying radii of rotation are shown in Fig. 3. Note, however, that the planar and SPECT FWHM values measured with a pixel size comparable to the spatial resolution are in error due to the low sampling frequency. In spite of this limitation, these results confirm the improvement to be gained in spatial resolution of SPECT images from the use of a larger matrix and a smaller radius of rotation. The 300-keV collimator displays the poorest SPECT FWHM values.
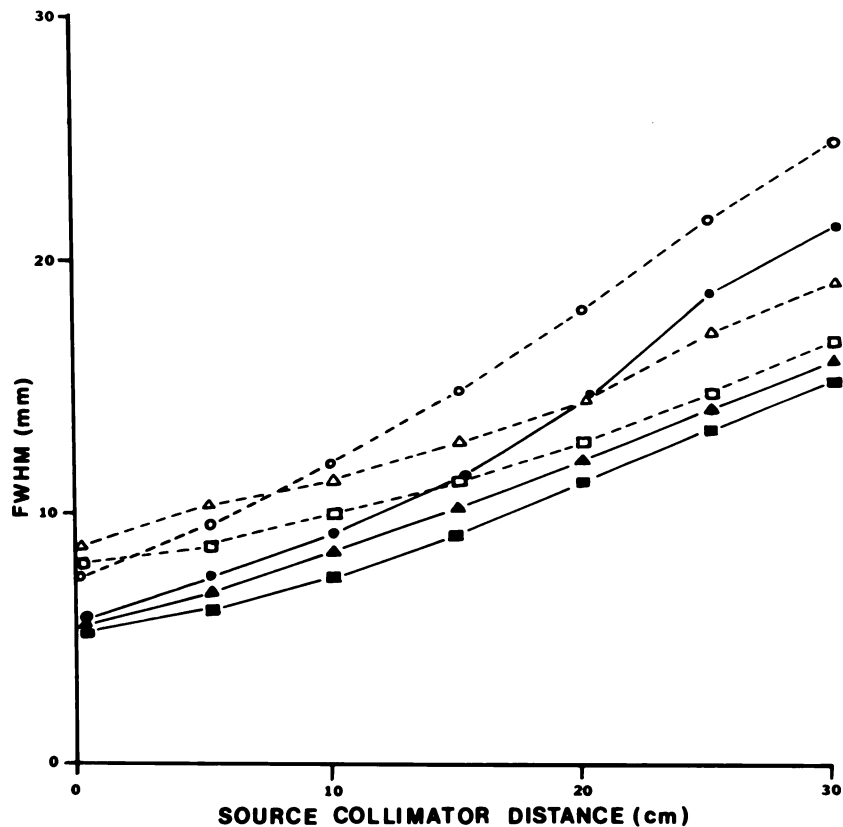
Planar images of the lucite rods in the SPECT phantom filled with ^{123}I(p,5n) are shown for each collimator in Fig. 4. The central area of the planar image of the cold rods in the SPECT phantom obtained with the low-energy collimators indicated a progressive increase in counts, and the clarity of visualization of the cold rods improved with distance from the center to the edge of the phantom. These results contradicted the superior spatial resolution obtained with the low-energy collimators and a line source in air.

As indicated by the count profiles through images obtained with the low-energy collimators, the lead disk failed to reduce to background levels the recorded counts from the uniform area of the SPECT phantom (Fig. 5). Note also the shape and size of the tails at the edge of the phantom. For the 300-keV collimator,

159-keV peak and background events recorded were used to find the "corrected" sensitivity values given in Table 2. The apparent sensitivity in Table 2 was found by the addition of peak and background events in the 159-keV peak defined with a symmetric 20% window. The peak to total ratio was defined as the peak to total counts in this 20%-energy window.

TABLE 2
Apparent (159-keV peak + background) and Corrected (159-keV peak) Sensitivities of Three Collimators for Small and Large Volume Source of ^{123}I(p,5n) at 10 cm in Air

| | Sensitivity cps μCi^{-1} | | | | | |
| Collimator type | 10-ml sphere | | | SPECT cylindrical phantom | | |
	Apparent	Corrected	Peak/total	Apparent	Corrected	Peak/total
LEAP	8.56	3.40	0.42	2.36	0.897	0.38
LEHRP	5.68	1.76	0.31	1.60	0.496	0.31
300 keV	2.69	1.88	0.70	0.98	0.500	0.51

FIGURE 2
Measured planar FWHM values for ^{123}I(p,5n) in air at various source-to-camera distances for each of three collimators using 64 × 64 (300 keV = O–O; LEAP-△–△; LEHRP-□–□) or 128 × 128 (300 keV-●—●; LEAP-▲—▲; LEHRP-■—■) matrix. 300-keV collimator demonstrated poorest resolution. Resolution was improved for each collimator when 128 × 128 matrix was used

however, the lead disk almost reduced the counts in the same area to background.

Transverse section images of the lucite rods in the SPECT phantom are shown in Fig. 6 for the three collimators. These indicate that the transverse section images obtained with the low-energy collimators studied in this report were seriously degraded by artifacts at the center of the field-of-view and the introduction of a rind of counts outside the direct area of the phantom. These artifacts probably result from septal penetration rather than center of rotation artifacts and are more likely the result of shifting uniformity artifacts introduced in the projection data images. A large proportion of the septal penetration events recorded with the low-energy collimators in the projection data images appear to be reduced to counts outside the phantom and lead to nonstationary artifacts at the center of the section image. Section images of the uniform area of the SPECT phantom are also similarly degraded as depicted in Fig. 7. The section images of the lucite rods and the uniform area of the SPECT phantom obtained with the 300-keV collimator were not degraded by artifacts, and depicted the usual progressive depression of counts with distance from section boundary due to photon attenuation which could be corrected with a linear attenuation coefficient (LAC) value of 0.12 cm^{-1}. Also shown in Fig. 6 is a transverse section image of the lucite rods in the SPECT phantom obtained with ^{99m}Tc and the LEHRP collimator. This illustrates the performance of the SPECT system in the absence of septal penetration.

DISCUSSION

The present studies indicate that planar and SPECT imaging of large volume sources of ^{123}I(p,5n) with low-energy collimators is complicated by septal penetration. In clinical studies septal penetration from sources out of the direct field-of-view can be even more complicated. One example is ^{123}I-labeled iodoamphetamine brain imaging where over 90% of the administered dose is in the lungs. Although the proportion of photons above 200 keV during ^{123}I decay is small, the distortion of planar and SPECT images is significant and even more pronounced in the presence of radionuclide contaminants induced by alternative ^{123}I production methods. Other problems related to the presence of these high-energy photons are the differences observed in uptake values measured with ^{123}I(p,2n) and iodine-131 (^{131}I), and the need for corrected calibration factors when ^{123}I is assayed in various containers using an ionization chamber (7,8). Satisfactory planar images and reasonable agreement with ^{131}I thyroid uptake values have been reported for ^{123}I(p,5n) even though septal penetration is increased by 13 to 20% when a 140-keV collimator is used for imaging a source emitting 159-keV photons (9).

The influence of septal penetration of low-energy collimators is seen principally as an isotropic but nonstationary distortion of planar image uniformity and the assignment of events outside the location of the source on the planar image. For any region of the
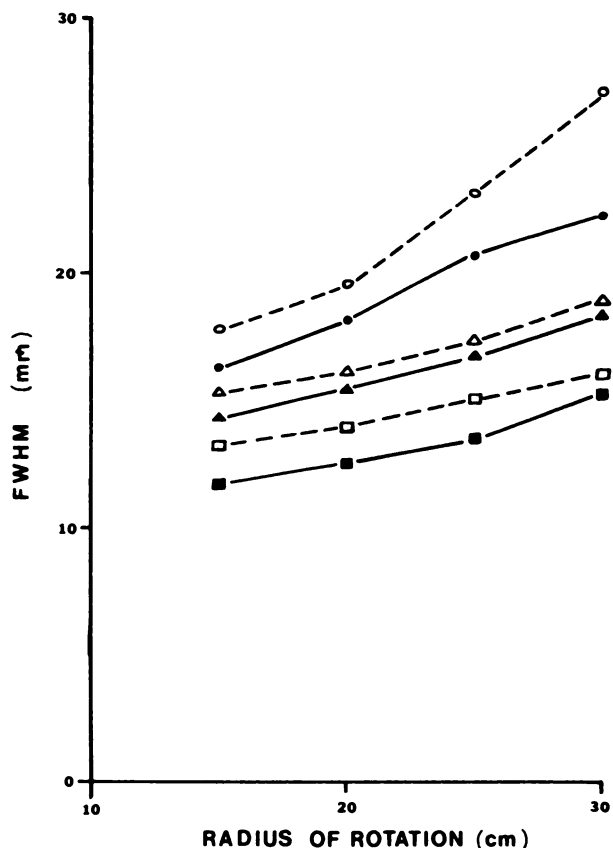
FIGURE 3

Measured SPECT FWHM values for [133]I(p,5n) line source in air at various radii of rotation (ROR) for each of three collimators using 64 × 64 (300 keV-O–O; LEAP-△–△; LEHRP-□–□) or 96 × 96 (300 keV-●—●; LEAP-▲—▲; LEHRP-■—■) matrix. Conclusions were analogous to those for Fig. 2. Degradation of resolution with increasing radius of rotation was most marked for 300-keV collimator

gamma camera crystal the number of photons contributing to the image consists of three types of events. First, primary 159-keV photons pass directly through the collimator holes together with higher energy pho-

tons that are scattered in the tissue surrounding the source or the detector. Second, high-energy photons penetrate the collimator septa and can interact with the same region of the detector at angles other than normal to the collimator direction. Third, high-energy photons penetrate the septa, produce Pb x-rays, bremsstrahlung and secondary electrons in the collimator material in close proximity to the detector, and are detected with high efficiency resulting in summation effects. We noticed that the [123]I(p,5n) gamma-ray spectra recorded with the low-energy collimators contained a significant Pb K shell x-ray peak at ~80 keV in contrast to the medium-energy collimator spectrum (Fig. 1). Note that the gamma camera crystal thickness will affect the Compton escape probability and change the recorded gamma-ray spectra.

When septal penetration is present with a large uniform flood source of [123]I(p,5n) that completely covers the camera field of view, every region of the camera crystal will receive a similar contribution of the three types of incident photons, so that a form of incident photon equilibrium will exist reflected by a uniform number of events detected in each area of the field-of-view. The resultant integral and differential uniformity values will, therefore, be similar to those obtained with a flood source of [99m]Tc. However, if the uniform source is imaged with only part of the field-of-view covered by the source, the incident photon equilibrium in every part of the crystal will be disturbed and observed as a significant deterioration in perceived uniformity. This makes it difficult to envisage how one could apply the usual uniformity correction method to planar images obtained with a low-energy collimator for [123]I(p,5n), particularly when the radionuclide distribution in an organ may only cover a small proportion of the total field-of-view of a gamma camera.

Planar and SPECT measurements of resolution in air suggested superior imaging performance of the low-energy collimators but was contradicted by the observed
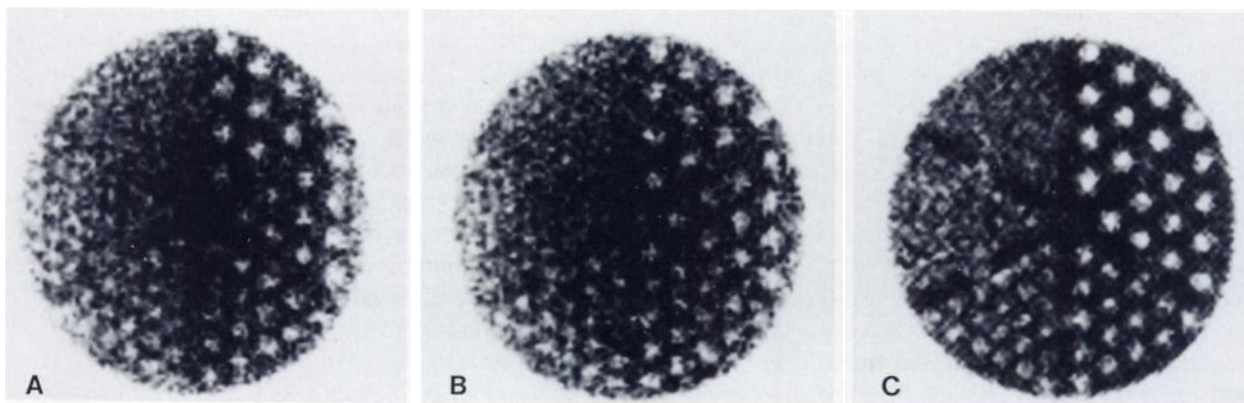

FIGURE 4

Planar images of lucite rods in SPECT phantom filled with [123]I(p,5n) recorded for 10^6 counts with each of three collimators (A) LEAP, (B) LEHRP, and (C) 300 keV. 300-keV collimator provided superior resolution of rods, particularly in center of phantom because of less interference by septal penetration
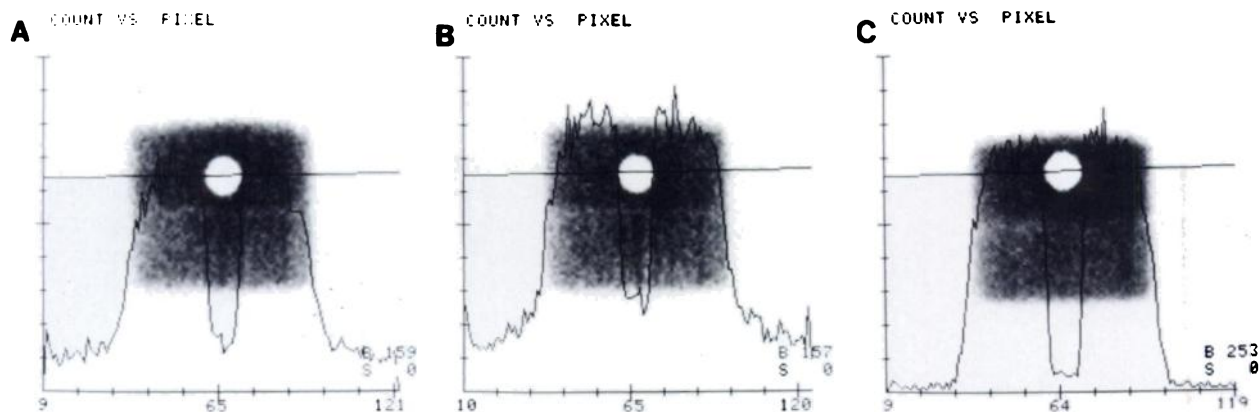
FIGURE 5
Planar images and count profiles of SPECT phantom filled with ¹²³I(p,5n) recorded for 10⁶ counts with each of three collimators (A) LEAP, (B) LEHRP, and (C) 300 keV. Lead disk was placed between collimator and uniform area of phantom. Count profiles indicate contribution of events arising from septal penetration under lead disk and outside direct image of phantom

planar and transverse section images of the SPECT phantom. These observations confirm and extend those of Bolmsjo (3). Discrepancies between our results and those reported by others (2,4,9,10) are more apparent than real and are influenced by differing physical char-

FIGURE 6
Transverse section images of lucite rods (diameter 4.8, 6.4, 7.9, 9.5, 11.1, 12.7 mm) in SPECT phantom filled with ¹²³I(p,5n). (A) LEAP—4.9 × 10⁶ counts, (B) LEHRP—3.2 × 10⁶ counts, and (C) 300 keV—1.9 × 10⁶ counts. Radius of rotation of 20 cm was used and each slice is 6.8 cm thick. Peripheral ring artifacts and distortion of counts were serious problems noticed with low-energy collimators. Also shown for comparison in (D) is transverse section image of lucite rods in phantom obtained with ⁹⁹ᵐTc and LEHRP collimator. Radius of rotation is 15 cm and section contains 1.5 × 10⁸ counts

acteristics of collimators, conditions of experiments and purity of ¹²³I.

Distortions in the planar images led on reconstruction to serious artifacts in the transverse section images. In section images of the SPECT phantom obtained with the low-energy collimators, the reduced count density outside of the phantom area, the presence of a more peripheral rind of increased count density and little reduction in counts in the central area of the section image were problems directly related to the distorted planar image uniformity artifacts. The resultant distorted section images make attenuation compensation inappropriate. The artifacts seen in the section images probably arise from the assumptions implicit in the reconstruction algorithm that all photons detected in any region of the camera image were incident normal to the camera face, i.e., they passed through the collimator holes. The observed transverse section count distribution does not correspond to projections of a physically realizable phantom. This is particularly noticeable for background areas outside the boundary of the phantom. Septal penetration events will, therefore, be incorrectly positioned in the reconstructed transverse section images.
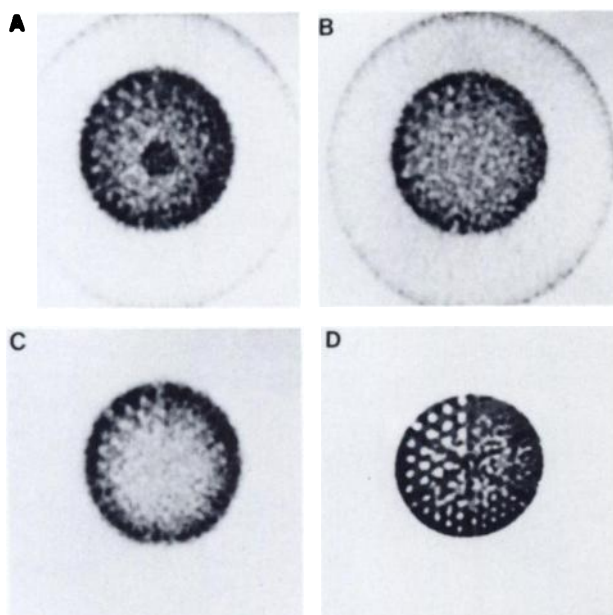
In any radionuclide investigation where ¹²³I uptake in an organ or site in the body is required, the sensitivity of the gamma camera-collimator combination will appear to be elevated due to septal penetration. The apparent planar sensitivity for each collimator for a small 10-ml volume source and the large SPECT phantom are given in Table 2. The apparent sensitivity values for the low-energy collimators appear elevated when compared to sensitivity measurements with ⁹⁹ᵐTc. Corrected ¹²³I sensitivity values were calculated for each collimator by estimating the peak to total count ratio of the photopeak counts recorded in the relevant gamma-ray spectrum. The corrected sensitivity values appear depressed compared with ⁹⁹ᵐTc partly because

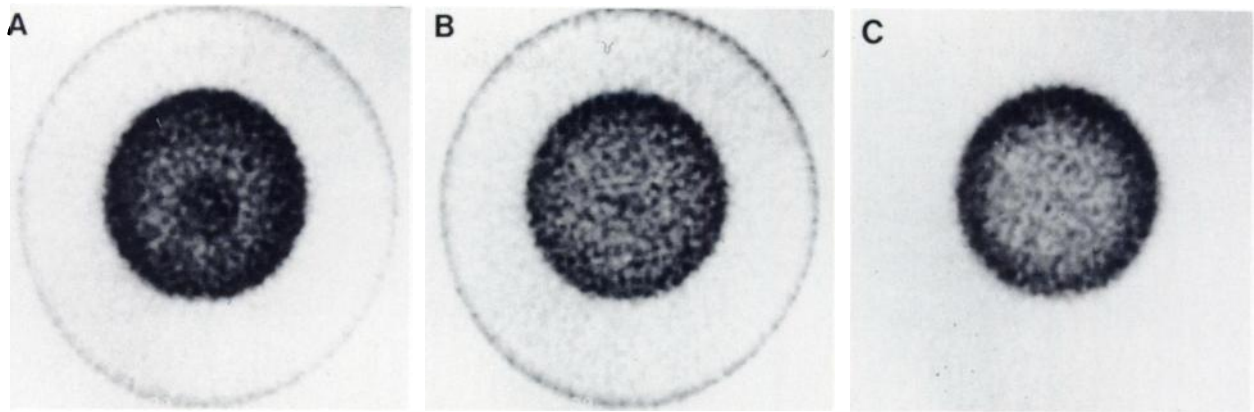## FIGURE 7

Transverse section images of uniform area of SPECT phantom filled with ^{123}I(p,5n), obtained with each of three collimators (A) LEAP, (B) LEHRP, and (C) 300 keV. In addition to peripheral and central artifacts, septal penetration in low-energy collimators almost obliterated effect of attenuation in these uncorrected images. In contrast, attenuation effect was present in image obtained with 300-keV collimator, and was confirmed by count profile

the simple linear interpolation method used underestimates the full-energy peak area. Measurements of ^{123}I uptake with planar images using low-energy collimators are likely to overestimate uptake if the radionuclide is widely distributed in the body, or underestimate if the uptake is highly localized.

Our conclusion from the present studies is that both planar and SPECT imaging of relatively large volume sources of ^{123}I(p,5n) using low-energy collimators is degraded by septal penetration to an extent that is not predicted by measurements of the FWHM. This differs from the conclusion reached from a comparison of the performance of low- and medium-energy collimator for tomographic imaging of ^{123}I(p,2n) contaminated with ^{124}I (10). The medium-energy collimator was found from the present results to be the preferred collimator for planar and SPECT imaging of ^{123}I(p,5n)-labeled antibodies in patients where quantitation of uptake in small and large volume sources is of interest (11). In clinical imaging with iodinated antibodies it can be difficult to obtain planar images with ~ 10^6 counts for a large organ such as the liver or 10^3 counts for a small tumor. At first glance the increased sensitivity of the low-energy collimators might appear more appropriate. However, statistical considerations indicate that even for the small lesion with 10^3 counts the 300-keV collimator image has a standard deviation of 4.3% compared with 4.4% for LEAP and 7.6% for LEHRP. In addition, the contrast for detection of the lesion is highest for the 300-keV collimator.

FOOTNOTES

ACKNOWLEDGMENTS

REFERENCES

1. McKeighen RE, Muehllehner G, Mayer RA: Gamma camera collimator considerations for imaging ^{131}I. *J Nucl Med* 15:328–331, 1974
2. Lagunas-Solar MC, Hines HH: Effects of radionuclidic composition on dosimetry and scintillation-imaging characteristics of ^{127}I(p,5n)-and ^{124}Te(p,2n)-made iodine-123 for nuclear medicine applications. In *The Developing Role of Short-Lived Radionuclides in Nuclear Medical Practice*, Paras P, Thiessen JW, eds. DOE CONF-820523, Washington, DC, Office of Scientific and Technical Information, United States Department of Energy, 1985, pp 423–444
3. Bolmsjo MS, Persson BRR, Strand SE: Imaging ^{123}I with a scintillation camera: A study of detection performance and quality factor concepts. *Phys Med Biol* 22; 266–277, 1977
4. Coleman RE, Greer KL, Drayer BP, et al: Collimation for I-123 imaging with SPECT. *Emission Computed Tomography—Current Trends*. Esser PD, ed. New York, NY, Society of Nuclear Medicine, pp 135–145, 1983
5. Siemens Technical Sheet of Collimators, Siemens, Des Plaines, IL, 1984
6. Chang LT: A method for attenuation correction in radionuclide computed tomography. *IEEE Trans Nucl Sci*, Vol 25, No 1, 1978, pp 638–643
7. Baker GA, Lum DJ, Smith EM, et al: Significance of radiocontaminants in ^{123}I for dosimetry and scintillation camera imaging. *J Nucl Med* 17:740–743, 1976
8. Johnston AS, Colombetti LG, Baker SI, et al: Dose calibrator readings due to radionuclidic impurities found in radiopharmaceuticals. *Nucl Med* 19:1–6, 1980
9. Denardo GL, Krohn KA, Jansholt A, et al: Present

and future applications of iodine-123. *Medical Radio-nuclide Imaging*, Vol 2, IAEA-SM-210/308, 1977, pp 3–20

10. Polak JF, English RJ, Holman BL: Performance of collimators used for tomographic imaging of I-123

contaminated with I-124. *J Nucl Med* 24:1065–1069, 1983

11. DeNardo GL, Raventos A, Hines HH, et al: Requirements for a treatment planning system for radioimmunotherapy. *Int J Radiat Biol* 11:335–348, 1985